In situ construction of WNiM-WNi LDH (M = Se, S, P) with heterointerfaces as highly efficient electrocatalyst for overall water splitting and urea oxidation reaction

Chenyi Zhang[a], Xiaoqiang Du[a*], Xiaoshuang Zhang[b] ,Yanhong Wang[a] and Tuoping Hu[a]

[a] School of Chemistry and Chemical Engineering, North University of China, Xueyuan road 3, Taiyuan 030051, People's Republic of China. E-mail: duxq16@nuc.edu.cn

[b] School of Environment and Safety Engineering, North University of China, Xueyuan road 3, Taiyuan 030051, People's Republic of China.

The same volume of gas sample in the headspace of the electrolytic cell was withdrawn by a SGE gas-tight syringe and analyzed by gas chromatography (GC). The O_2 in the sampled gas was separated by passing through a 2 m × 3 mm packed molecular sieve 5A column with an Ar carrier gas and quantified by a Thermal Conductivity Detector (TCD)(Shimadzu GC-9A).

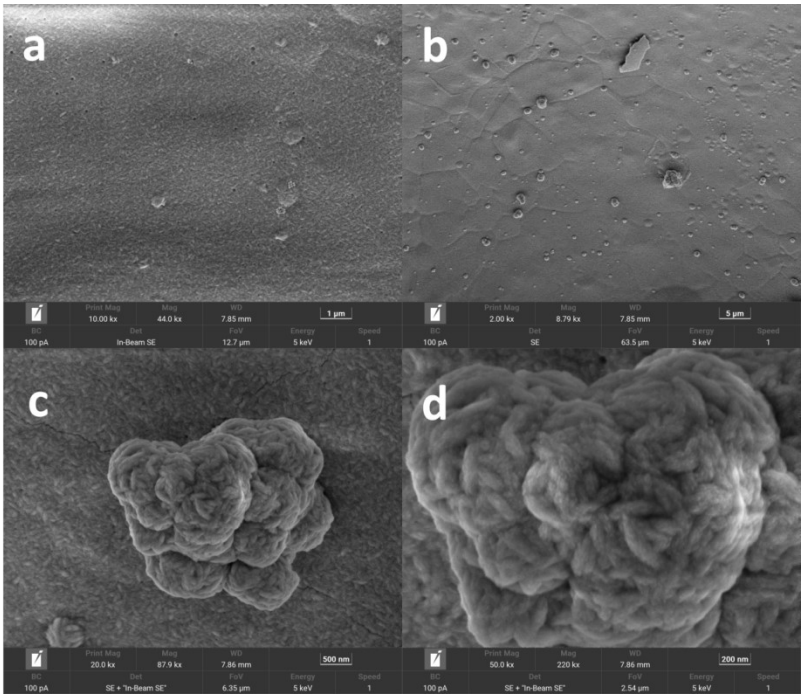

Fig. S1 (a–d) Typical SEM images of the WN LDH on Ni foam.

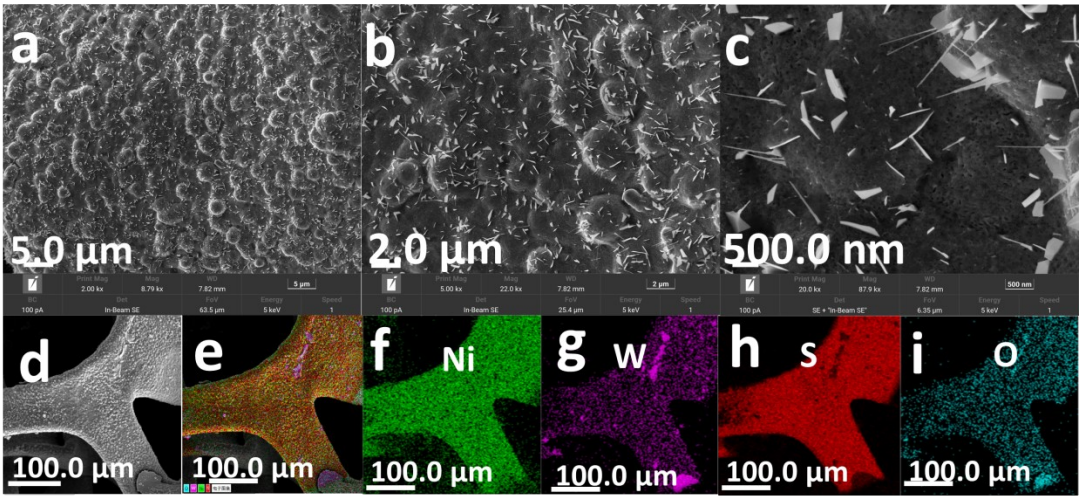

Fig. S2 (a–c) Typical SEM images of the WNS/WN LDH on Ni foam; (d-i) EDX element mapping of Ni, W, S, and O.

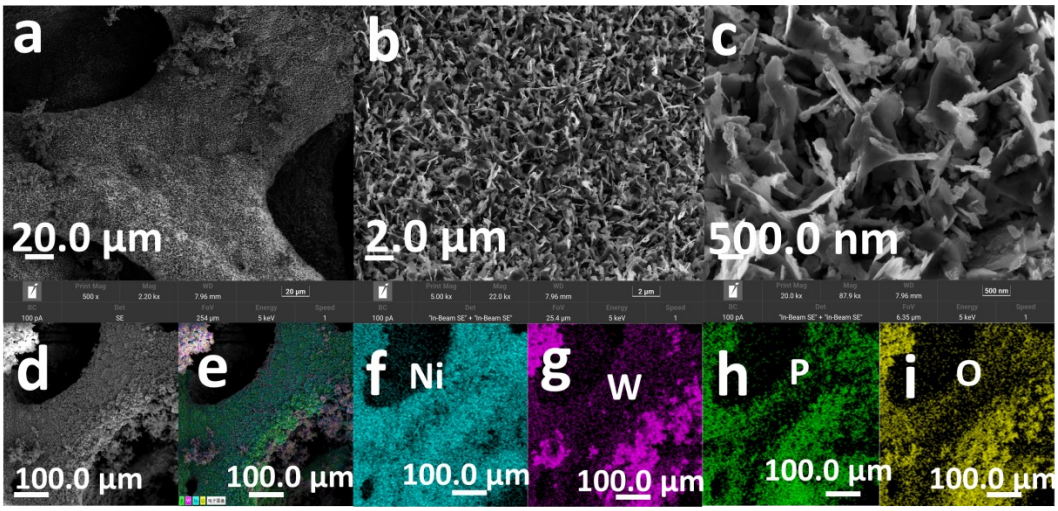

Fig. S3 (a–c) Typical SEM images of the WNP/WN LDH on Ni foam; (d-i) EDX element mapping of Ni, W, P, and O.

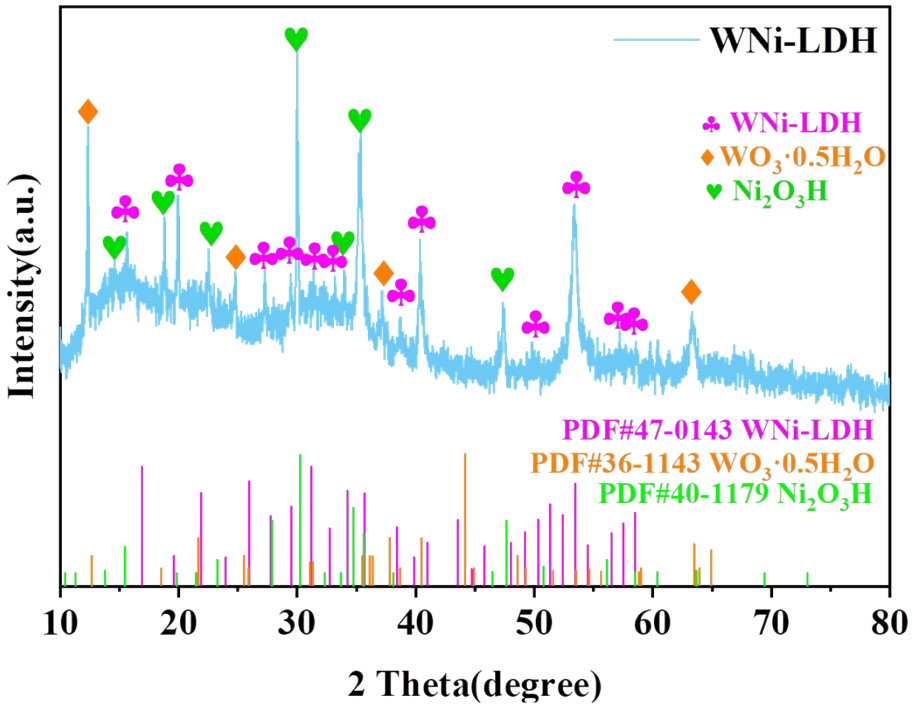

Fig. S4 (a) XRD pattern of the WN LDH nanoarrays.

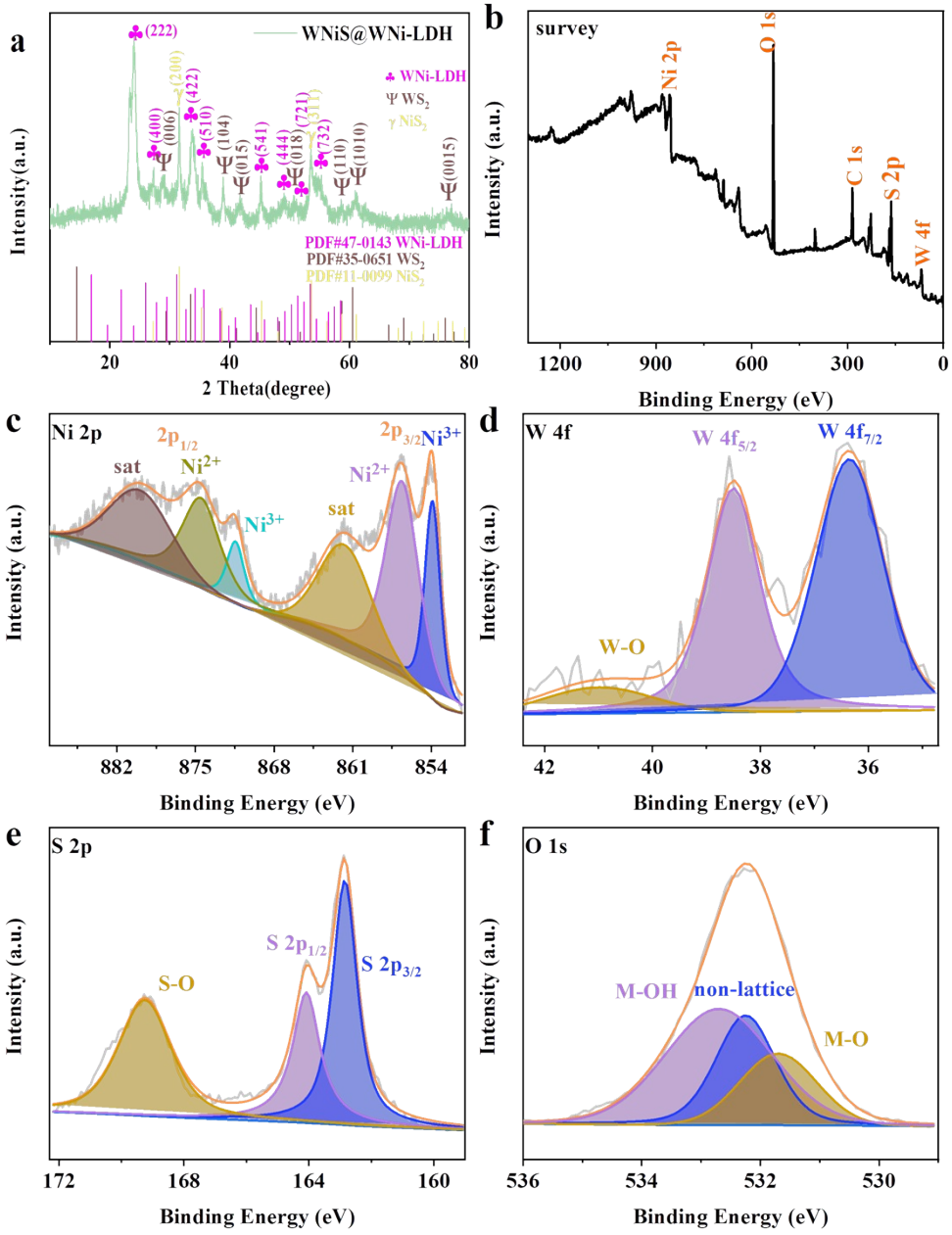

Fig. S5 (a) XRD pattern; XPS of (b) survey, (c) high-resolution Ni 2p, (d) W 4f, (e) S 2p and (f) O 1s spectra of the WNS-WN LDH nanoarrays.

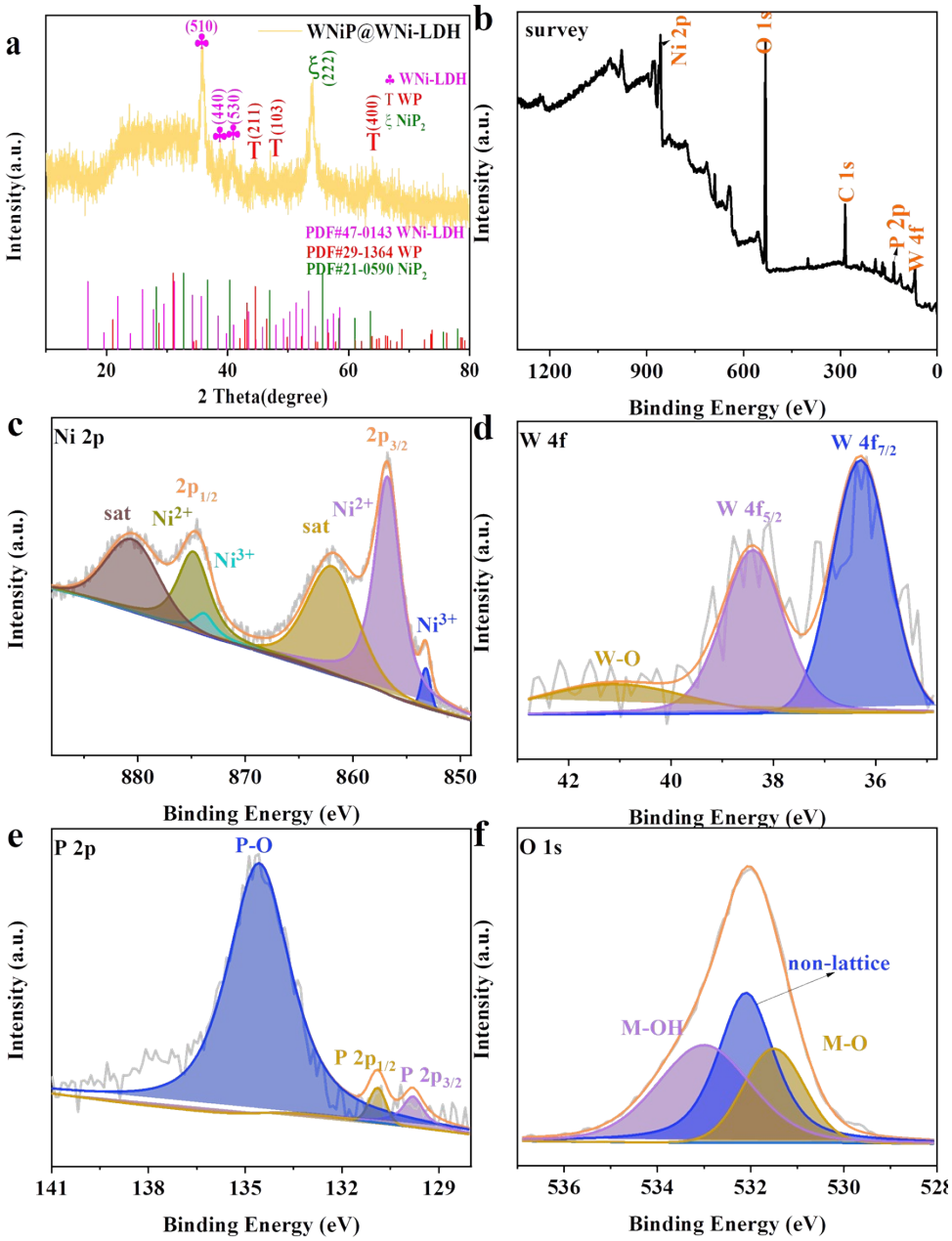

Fig. S6 (a) XRD pattern; XPS of (b) survey, (c) high-resolution Ni 2p, (d) W 4f, (e) P 2p and (f) O 1s spectra of the WNP-WN LDH nanoarrays.

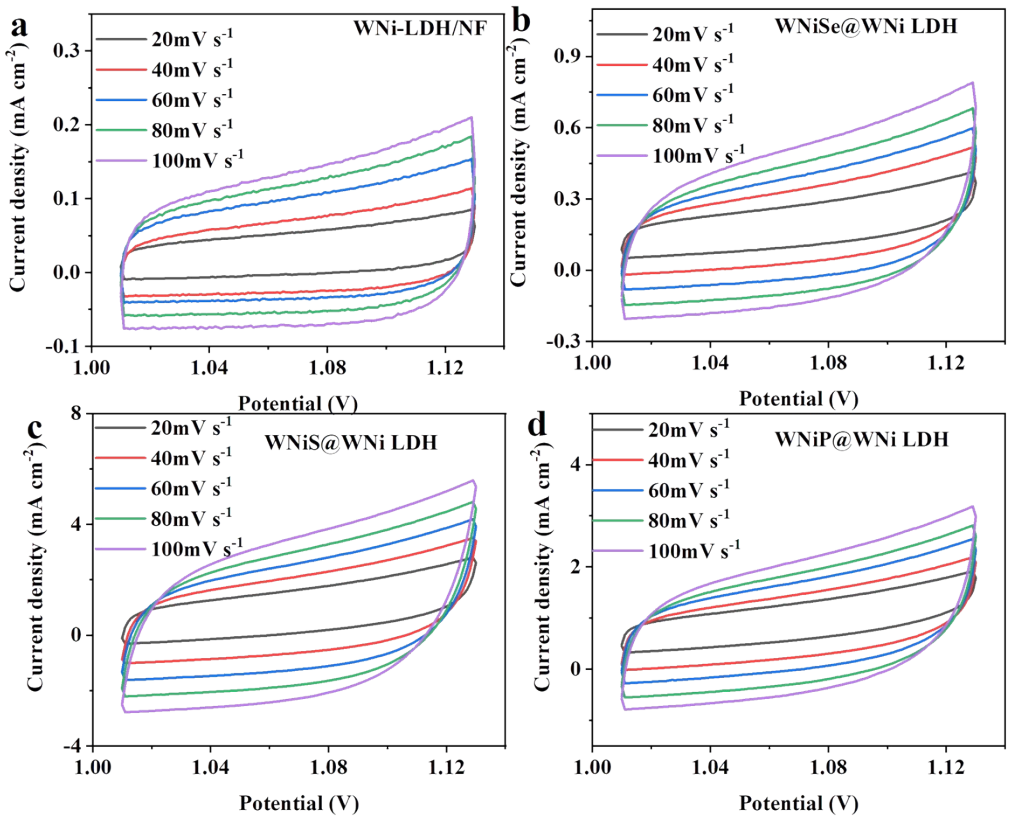

Fig. S7. In 1.0 M KOH, OER cyclic voltammograms of a) WNi LDH/NF, b) WNiSe@WNi LDH/NF, c) WNiS@WNi LDH/NF and d) WNiP@WNi LDH/NF at the different scan rates varying from 20 to 100 $mV \cdot s^{-1}$.

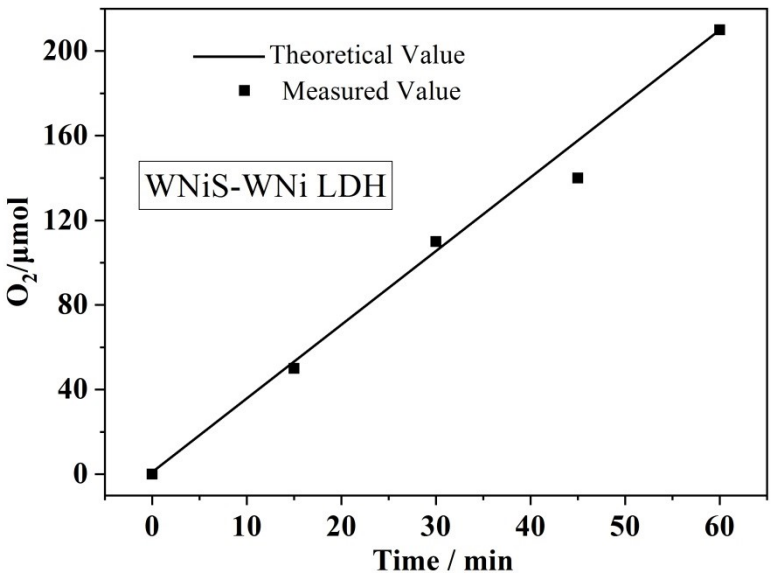

Fig. S8 Electrocatalytic efficiency of O_2 production over WNiS@WNi LDH/NF.

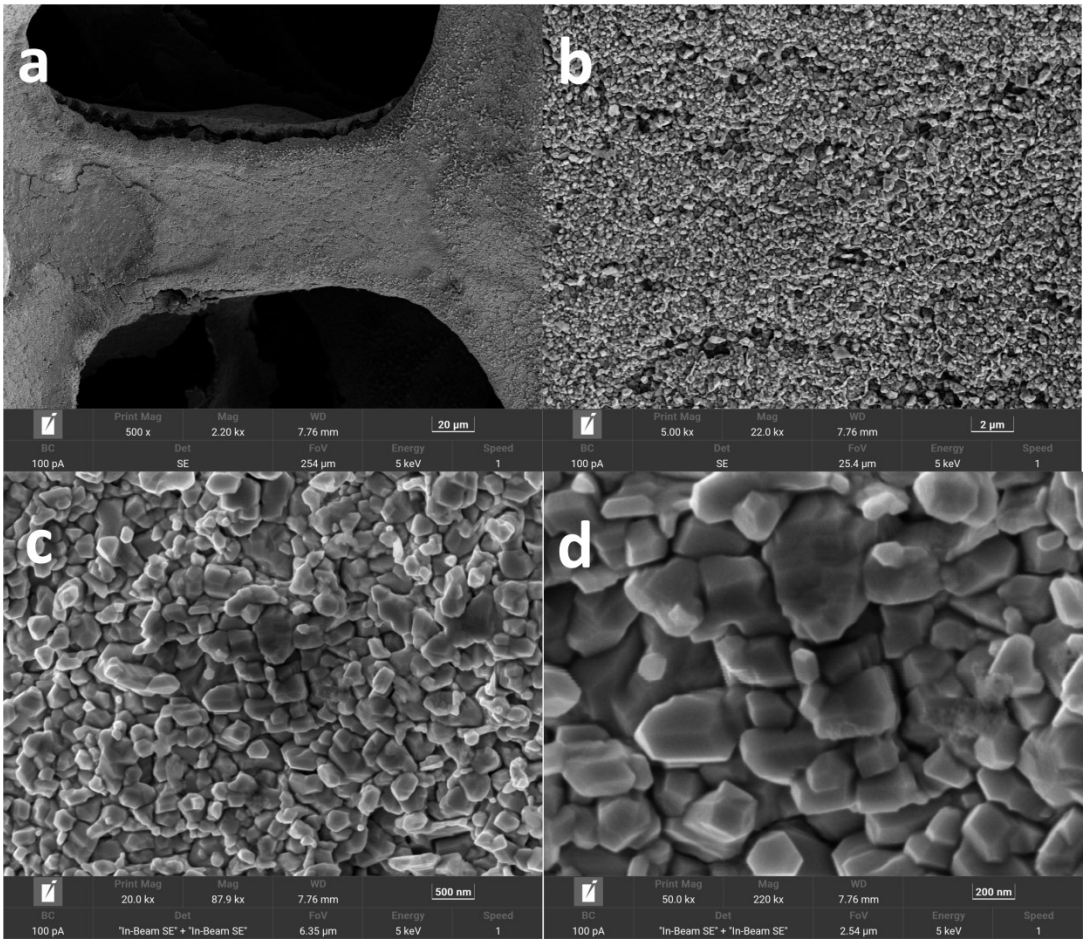

Fig. S9 SEM of WNiS@WNi LDH/NF after 12 h for OER.

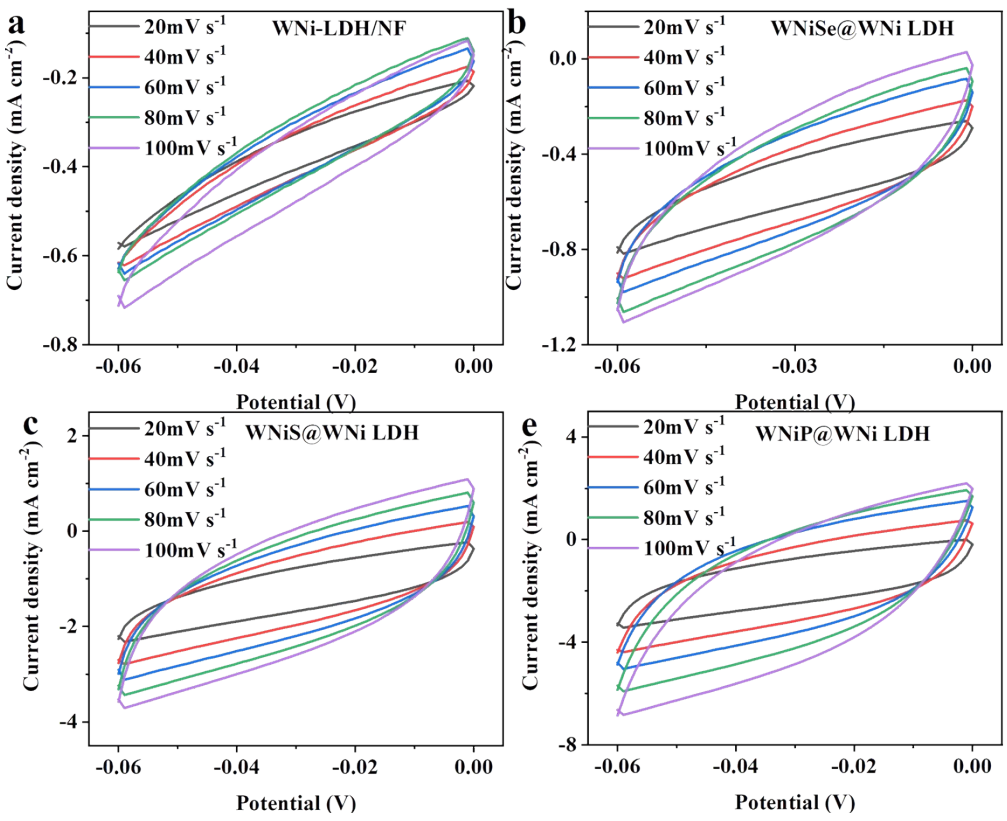

Fig. S10. In 1.0 M KOH, HER cyclic voltammograms of a) WNi LDH/NF, b) WNiSe@WNi LDH/NF, c) WNiS@WNi LDH/NF and d) WNiP@WNi LDH/NF at the different scan rates varying from 20 to 100 $mV \cdot s^{-1}$.

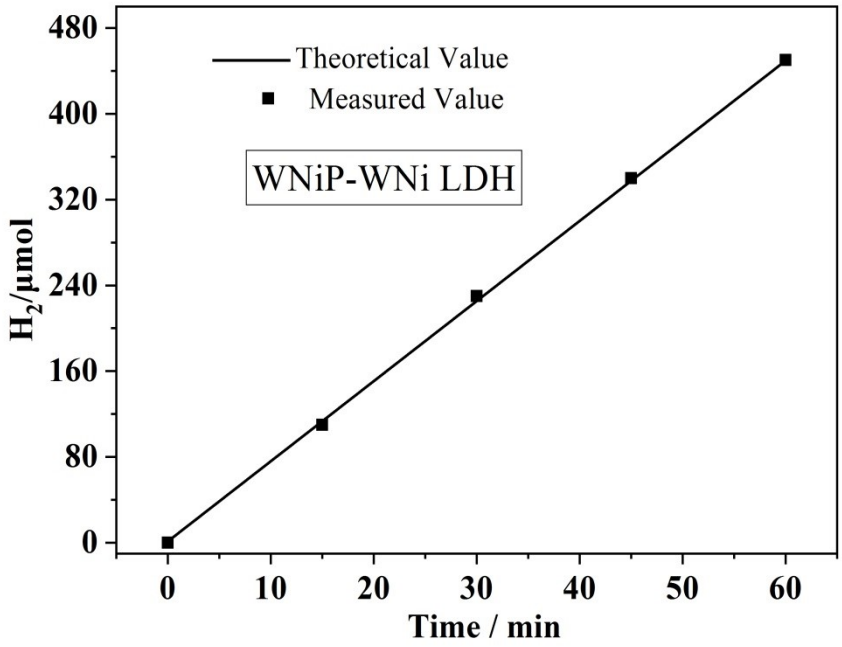

Fig. S11 Electrocatalytic efficiency of H_2 production over WNiP@WNi LDH/NF.

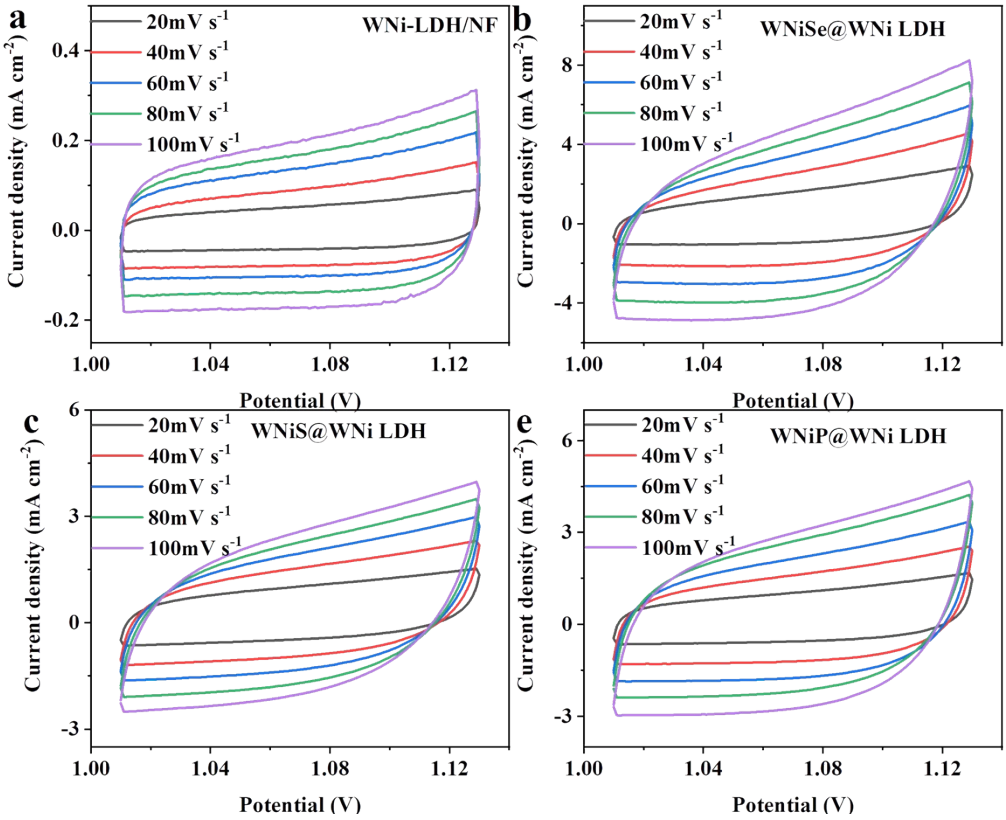

Fig. S12. In 1.0 M KOH with 0.5 M urea, UOR cyclic voltammograms of a) WNi LDH/NF, b) WNiSe@WNi LDH/NF, c) WNiS@WNi LDH/NF and d) WNiP@WNi LDH/NF at the different scan rates varying from 20 to 100 $mV \cdot s^{-1}$.

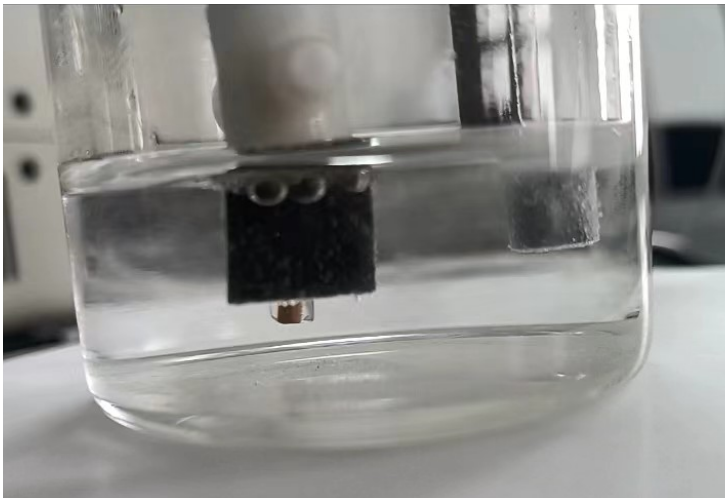

Fig. S13 The physical image of H_2 and O_2.

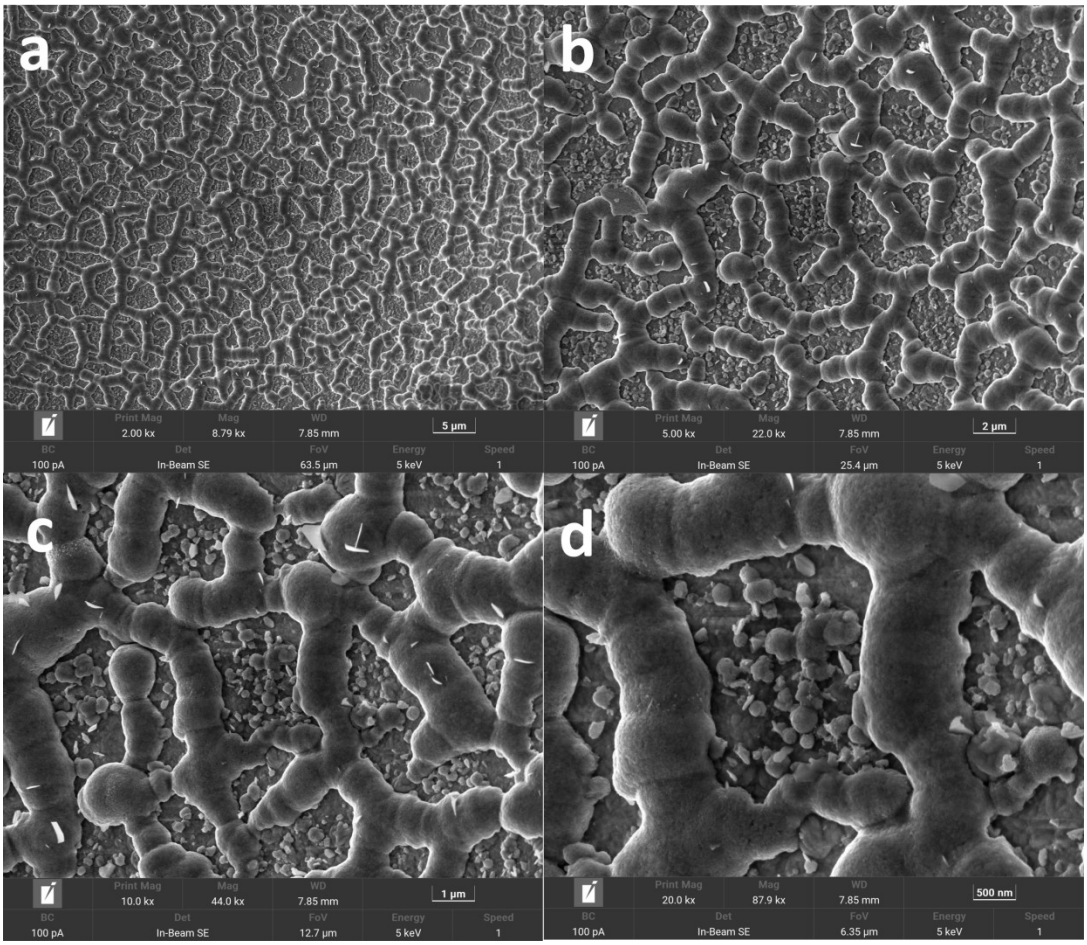

Fig. S14 SEM of WNiSe@WNi LDH/NF after 12 h for UOR.

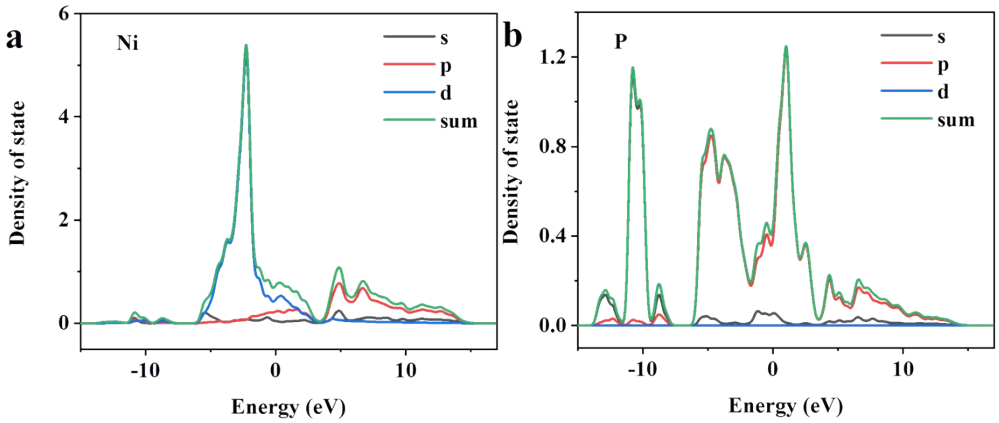

Fig.S15 Density of states for the NiP_2, (a) Ni and (b) P.

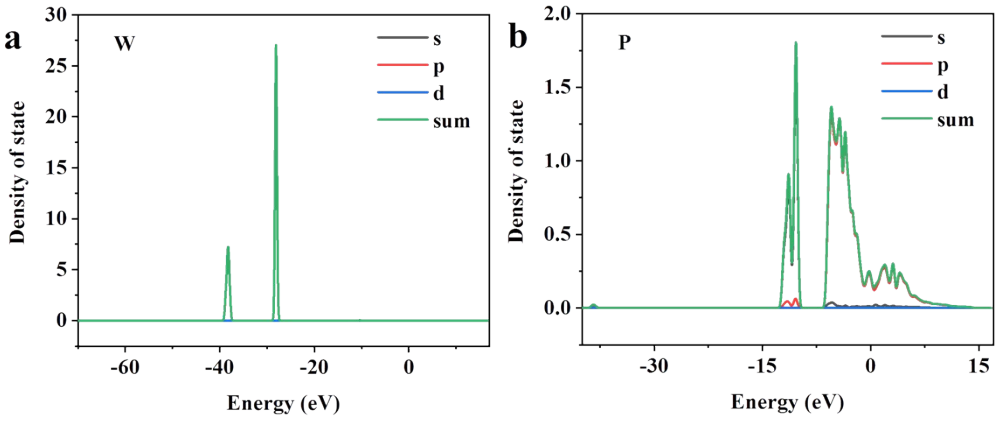

Fig.S16 Density of states for the WP, (a) W and (b) P.

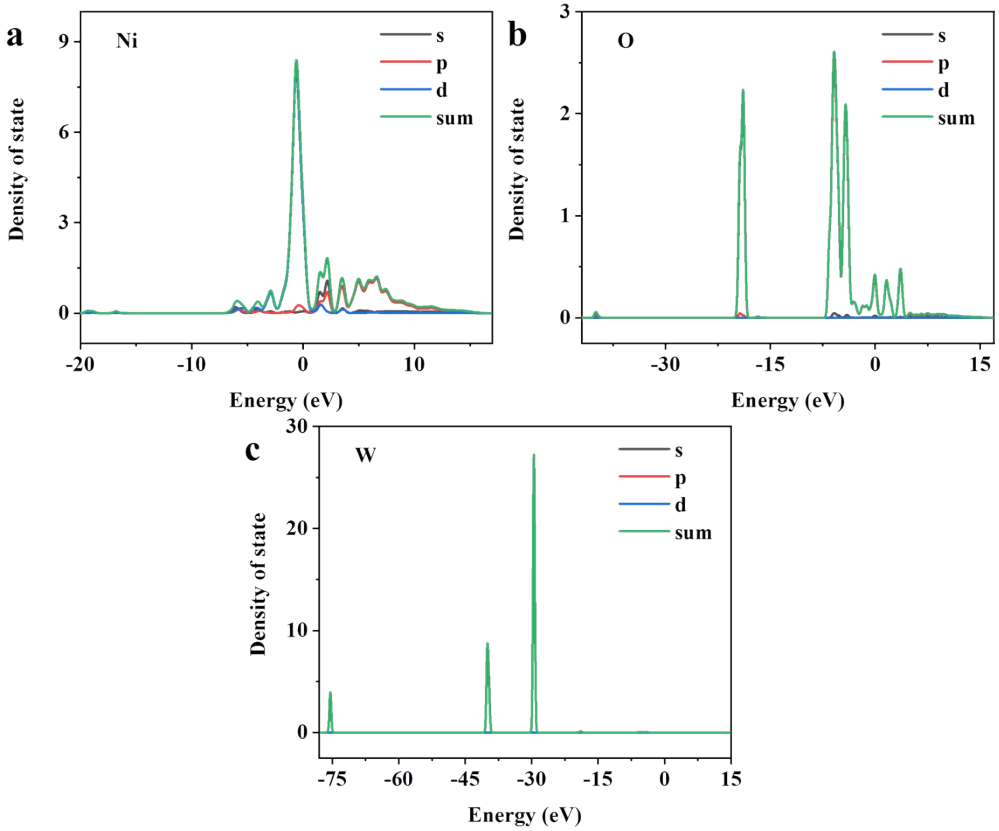

Fig.S17 Density of states for the WNi-LDH, (a) Ni, (b) O and (c) W.

Supplementary Table

Table S1. Comparison of OER activity for various catalysts

Catalyst	η(mV) at 10 mA/cm^2	electrolyte	References
WNiS-WNi LDH	64	1.0 M KOH	This work
NiFe LDH@NiCoP/NF	220	1.0 M KOH	[1]
Fe-Ni LDH/MOF-b2	255	1.0 M KOH	[2]
Fe-doped Co-Mo-S	268	1.0 M KOH	[3]
CoP/Ni_2P@HPNCP	294	1.0 M KOH	[4]
Ni_3B/Fe_2O_3	162	1.0 M KOH	[5]

Table S2. Comparison of HER activity for various catalysts

Catalyst	η(mV) at 10 mA/cm^2	electrolyte	References
WNiP-WNi LDH	126	1.0 M KOH	This work
$Co_5Mo_{1.0}P$ NSs@NF	173	1.0 M KOH	[6]
MoP@NPC/rGO	218	1.0 M KOH	[7]
Ni-Fe-P	182	1.0 M KOH	[8]
Ni_3S_2	170	1.0 M KOH	[9]
NiS_2	150	1.0 M KOH	[10]
Co@N–C	210	1.0 M KOH	[11]

Table S3. Comparison of UOR activity for various catalysts

Catalyst	V(V) at 10 mA/cm^2	electrolyte	References
WNiSe-WNi LDH	1.25	1.0 M KOH	This work
MoNiFeS_x@$FeNi_3$	1.31	1.0 M KOH	[12]
CoS_x/Co-MOF||CoS_x/Co-MOF	1.48	1.0 M KOH	[13]
NiFe-LDH	1.39	1.0 M KOH	[14]
Ni_2P/Fe_2P/NF	1.36	1.0 M KOH	[15]
$Ni_{0.9}Fe_{0.1}$Ox	1.455	1.0 M KOH	[16]

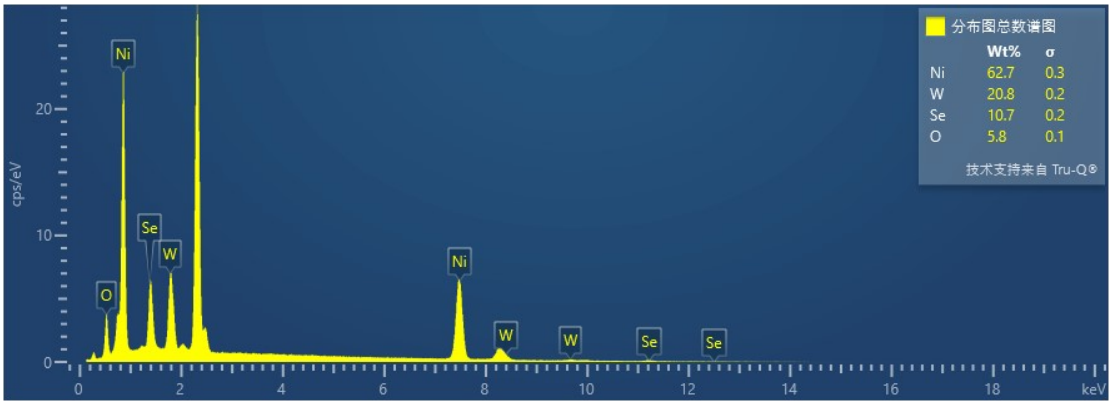

Element	Mass fraction %	Atomic fraction %
Ni	3.83	9.6
O	52.73	48.97
Se	1.77	1.08
W	1.29	1.16

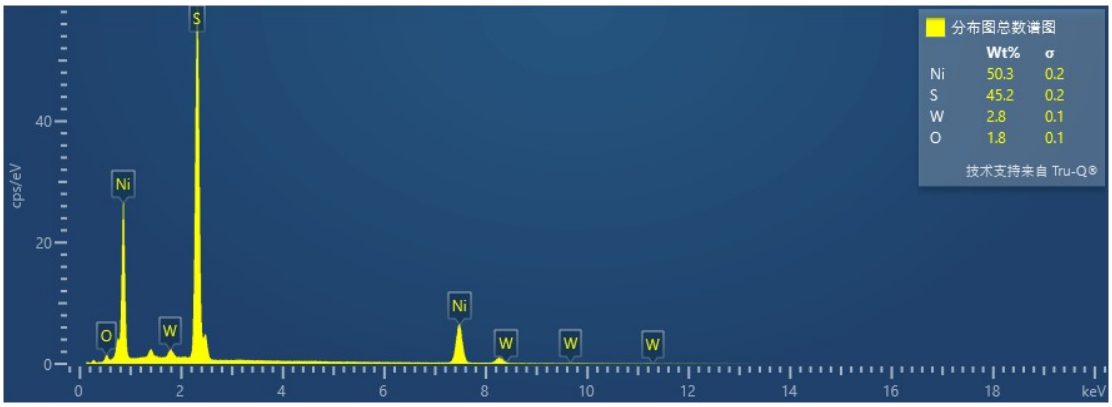

Element	Mass fraction %	Atomic fraction %
Ni	2.06	9.49
O	44.93	37.37
S	22.93	25.12
W	0.33	0.39

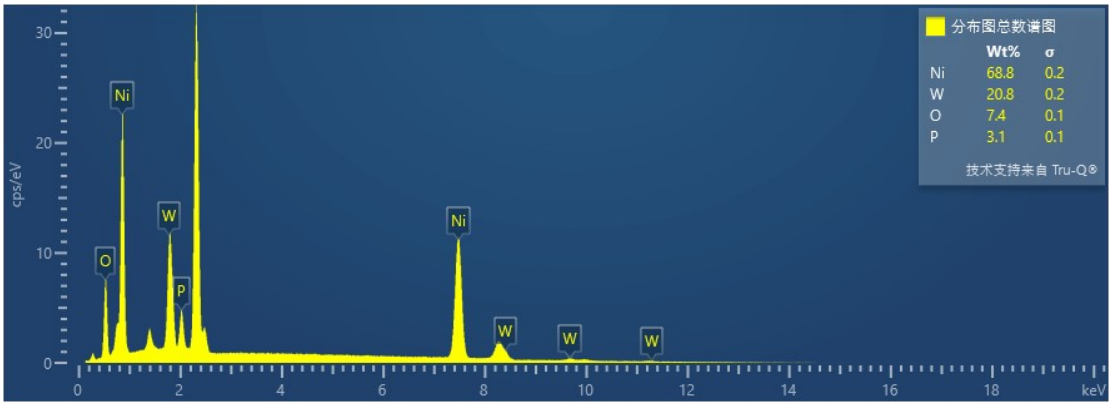

Element	Mass fraction %	Atomic fraction %

Ni	4.78	15.49
O	50.24	46.18
P	8.91	9.42
W	0.25	0.27

[1] H. Zhang, X. Li, A. Haehnel, V. Naumann, C. Lin, S. Azimi, S.L. Schweizer, A.W. Maijenburg, R.B. Wehrspohn, Bifunctional Heterostructure Assembly of NiFe LDH Nanosheets on NiCoP Nanowires for Highly Efficient and Stable Overall Water Splitting, Adv. Funct. Mater., 28 (2018).

[2] J. Huo, Y. Wang, L. Yan, Y. Xue, S. Li, M. Hu, Y. Jiang, Q.-G. Zhai, In situsemi-transformation from heterometallic MOFs to Fe-Ni LDH/MOF hierarchical architectures for boosted oxygen evolution reaction, Nanoscale, 12 (2020) 14514-14523.

[3] F. Yuan, Z. Liu, G. Qin, Y. Ni, Fe-Doped Co-Mo-S microtube: a highly efficient bifunctional electrocatalyst for overall water splitting in alkaline solution, Dalton Trans., 49 (2020) 15009-15022.

[4] R. Zhang, R. Zhu, Y. Li, Z. Hui, Y. Song, Y. Cheng, J. Lu, CoP and Ni2P implanted in a hollow porous N-doped carbon polyhedron for pH universal hydrogen evolution reaction and alkaline overall water splitting, Nanoscale, 12 (2020) 23851-23858.

[5] H. Zhao, M. Jiang, Q. Kang, L. Liu, N. Zhang, P. Wang, F. Zhou, Electrocatalytic oxygen and hydrogen evolution reactions at Ni3B/Fe2O3 nanotube arrays under visible light radiation, Catal. Sci. Technol., 10 (2020) 8305-8313.

[6] Y. Zhang, Q. Shao, S. Long, X.Q. Huang, Cobalt-molybdenum nanosheet arrays as highly efficient and stable earth-abundant electrocatalysts for overall water splitting, Nano. Energy., 45 (2018) 448-455.

[7] J.S. Li, J.Q. Sha, B. Du, B. Tang, Highly efficient hydrogen evolution electrocatalysts based on coupled molybdenum phosphide and reduced graphene oxide derived from MOFs, Chem. Commun., 53 (2017) 12576-12579.

[8] C.J. Xuan, J. Wang, W.W. Xia, Z.K. Peng, Z.X. Wu, W. Lei, K.D. Xia, H.L.L. Xin, D.L. Wang, Porous Structured Ni-Fe-P Nanocubes Derived from a Prussian Blue Analogue as an Electrocatalyst for Efficient Overall Water Splitting, ACS Appl. Mate. Inter., 9 (2017) 26134-26142.

[9] L.L. Feng, G.T. Yu, Y.Y. Wu, G.D. Li, H. Li, Y.H. Sun, T. Asefa, W. Chen, X.X. Zou, High-Index Faceted Ni3S2 Nanosheet Arrays as Highly Active and Ultrastable Electrocatalysts for Water Splitting, J. Am. Chem. Soc., 137 (2015) 14023-14026.

[10] X.L. Wu, B. Yang, Z.J. Li, L.C. Lei, X.W. Zhang, Synthesis of supported vertical NiS2 nanosheets for hydrogen evolution reaction in acidic and alkaline solution, Rsc Advances, 5 (2015) 32976-32982.

[11] J. Wang, D.F. Gao, G.X. Wang, S. Miao, H.H. Wu, J.Y. Li, X.H. Bao, Cobalt nanoparticles

encapsulated in nitrogen-doped carbon as a bifunctional catalyst for water electrolysis, J. Mater. Chem. A, 2 (2014) 20067-20074.
[12] Q. Li, W.X. Zhang, J. Shen, X.Y. Zhang, Z. Liu, J.Q. Liu, Trimetallic nanoplate arrays of Ni-Fe-Mo sulfide on FeNi3 foam: A highly efficient and bifunctional electrocatalyst for overall water splitting, J. Alloy. Compd., 902 (2022).
[13] H.Z. Xu, K. Ye, K. Zhu, J.L. Yin, J. Yan, G.L. Wang, D.X. Cao, Template-directed assembly of urchin-like CoSx/Co-MOF as an efficient bifunctional electrocatalyst for overall water and urea electrolysis, Inorg. Chem. Front., 7 (2020) 2602-2610.
[14] C.Y. Zhang, T.T. Chen, H. Zhang, Z.H. Li, J.C. Hao, Hydrated-Metal-Halide-Based Deep-Eutectic-Solvent-Mediated NiFe Layered Double Hydroxide: An Excellent Electrocatalyst for Urea Electrolysis and Water Splitting, Chem-Asian. J., 14 (2019) 2995-3002.
[15] L. Yan, Y.L. Sun, E.L. Hu, J.Q. Ning, Y.J. Zhong, Z.Y. Zhang, Y. Hu, Facile in-situ growth of Ni2P/Fe2P nanohybrids on Ni foam for highly efficient urea electrolysis, J. Colloid Interf. Sci., 541 (2019) 279-286.
[16] F.C. Wu, G. Ou, J. Yang, H.N. Li, Y.X. Gao, F.M. Chen, Y. Wang, Y.M. Shi, Bifunctional nickel oxide-based nanosheets for highly efficient overall urea splitting, Chem. Commun., 55 (2019) 6555-6558.